

Internal ballistics of polygonal and grooved barrels: A comparative study

Science Progress

2021, Vol. 104(2) 1–23

© The Author(s) 2021

Article reuse guidelines:

sagepub.com/journals-permissions

DOI: 10.1177/00368504211016954

journals.sagepub.com/home/sci

Usiel S Silva-Rivera¹ , Luis Adrian Zúñiga-Avilés^{1,2} , Adriana H Vilchis-González¹, Pedro A Tamayo-Meza³  and Wilbert David Wong-Angel⁴

¹Universidad Autónoma del Estado de México, Toluca, México

²Cátedras CONACYT, Facultad de ingeniería, UAEM, Ciudad universitaria, Toluca, México

³Instituto Politecnico Nacional, SEPI-ESIME U.P., Azcapotzalco, Ciudad de México, México

⁴Instituto Politécnico Nacional, SEPI-ESIME U.P., Zacatenco, Ciudad de México, México

Abstract

As a parameter important ballistic, the research about polygonal and grooved barrels' behavior has not been widely carried out. The pressures, velocities, stresses, deformations, and strains generated by the firing of 9 mm × 19 mm ammunition in weapons with polygonal barrels are analyzed numerically and experimentally, compared with those generated in pistols with grooved barrels. The Finite Element Method with equal boundary and loading conditions was used in both types of guns, specifying the actual materials of the projectile and the barrels. Subsequently, experimental tests were carried out on various weapons with 9 mm ammunitions of 115, 122, and 124 gr. The results show that the 9 mm bullet fired in a polygonal barrel undergoes a maximum deformation towards its exterior of 0.178 mm and interior of 0.158 mm, with stress up to 295.85 MPa. Compared with 0.025 mm maximum external deformation and 0.112 mm internal deformation of 9 mm projectiles fired in a grooved barrel, with stress up to 269.79 MPa. The deformation in the polygonal barrel is in a greater area, but the rifling impression left is less deep, making its identification more difficult. Although there are differences in the stresses and strains obtained, similar velocity and pressure parameters are achieved in the two types of barrels. This has application in the development and standardization of new kinds of barrels and weapons.

Keywords

Polygonal rifling, groove rifling, impression on fired bullets, transient analysis

Corresponding author:

Luis A Zúñiga-Avilés, Universidad Autónoma del Estado de México, Instituto Literario 100, Col. Centro, Toluca 50000, México.

Email: lazunigaa@uaemex.mx



Creative Commons Non Commercial CC BY-NC: This article is distributed under the terms of the Creative Commons Attribution-NonCommercial 4.0 License (<https://creativecommons.org/licenses/by-nc/4.0/>)

which permits non-commercial use, reproduction and distribution of the work without further permission provided the original work is attributed as specified on the SAGE and Open Access pages (<https://us.sagepub.com/en-us/nam/open-access-at-sage>).

Introduction

The ballistic analysis of pressure, velocity, heat transfer, stress, and deformation that are generated in the firing cycle of a firearm, is a relevant topic not only for the interaction of the projectile and the weapon but for the safety that it implies. The nonlinear finite element, orthogonal test method, and rigid body dynamics have been used to determine that the clearance between projectile and bore.¹⁻⁴

In the analysis of the dynamic process of firing, it has been determined that the deformation and dynamic response of a guided projectile is affected by the engraving force.^{5,6} Procházka and Ninh⁷ determined that a high temperature in the barrel walls causes more deformation than the mechanical load of the shot. The time-dependent heat flux and thermal stress in the multilayer barrel have been analyzed by Lee et al.⁸ The heat transfer coefficients with a thermo-mechanical approach have been studied.^{9,10} Suchocki and Ewertowski¹¹ defined that the recoil of a pistol P-64 does not have a significant influence on the accuracy of a single shot.

Deng et al.¹² obtained the rifling impression on the bullets after being fired with output times of 450 μ s (0.45 ms). Taraszewski and Ewertowski¹³ analyzed the interaction of the shooter with the rifle firings and obtained the force of the weapon's movement in the first 2 ms. Silva-Rivera et al.^{14,15} analyzed projectiles with partial core and got projectile output values close to 2 ms using ammunition caliber 7.62 mm \times 51 mm. Moreover, in other calibers, there are times of 8–9 ms for 20 mm cannons with barrels of one 524 mm (5 ft).¹⁶

The aforementioned studies were carried out in groove rifling barrels, so analysis in polygonal barrels is necessary. Glock and IWI manufacture polygonal barrels of six sides, and the Glock Gen five has a polygonal barrel of eight sides.¹⁷ Some authors consider that the bullet has a better fit in the polygonal barrels.¹⁸

Banno et al.¹⁹ in 2004 indicated that the appearance of the striations observed through optical devices might vary depending on the lighting. The deformation that the polygonal barrels cause to the projectiles is even less. In the 90's Glock implemented the Electronic Spark Reduction Method (ESRM) and in 2003 presented the Enhanced Bullet Identification System (EBIS).²⁰ However, there are still problems with their identification. Christen and Jordi²¹ determined the marks on the projectiles can be sufficient quality to correlate the projectiles fired with a firearm.

All these studies are affected by the weapons and ammunitions that exist for a single caliber. Only in the 9 mm \times 19 mm ammunition type Full Metal Jacket, there is the Parabellum bullet with the STANAG-4090²² and MIL-C-70508²³ standards, as well as the Luger and Luger + P bullet, with the specification SAAMI.²⁴

This study aims to determine the differences between bullets fired in hexagonal and conventional rifling barrels, considering the deformation, strain, and stress they are subjected to and the ballistic aspects of pressure and velocity. This is significant because the variation between these types of barrels is determined, and their operation is shown numerically and experimentally. Also, the numerical simulation carried out, and the results from this research increase the existing information on the operation of the polygonal barrels, how they could be improved and standardized. Additionally, it has application in the development of new types of

Table 1. Specifications of the used weapons.

Corp.	Std barrel	CZ	Sig Sauer	Ruger	Israel Weapon Industries (IWI)		
Model	9 mm	P-09	P 320	P 89	Jericho	Masada	Masada
Type	Six grooves	Six grooves	Six grooves	Six grooves	Six sides	Six sides	Six sides
Length (mm)	200	111.30	116.00	110.40	111.80	100.20	100.00

weapons, since the data can be extrapolated to new calibers, ammunitions, and barrels.

Materials and methods

In this research, the internal ballistics of the firing in polygonal and grooved barrels was analyzed. The numerical simulation was performed with two CAD models of 9 mm \times 19 mm barrels. The first model with a hexagonal profile, and the second model with six grooves, in both cases, having one turn in 10".

For the most reliable results, CAD models were made, taking into account measures of the Parabellum bullet, chamber, grooved barrel, breech bolt, and free-flight area, according to STANAG-4090 standard.²² Also, this standard was considered for the case of the hexagonal rifling barrel, concerning the weapon chamber and the turn length of the rifling, as well as actual measurements of the barrels for their internal shape.

The experimental tests carried out were of three types; first of pressure and velocity in a standardized barrel, second of velocity in polygonal and conventional pistol barrels, and third of dimensional measurements of the bullets fired and the barrels of the weapons.

Table 1 describes the weapons used; one standardized grooved barrel, three guns with groove rifling barrel, and three guns with a polygonal rifling barrel. At the indicated barrel length, the external geometry of some models and the space of the breech bolt was not considered. The pistols used are from the companies Česká Zbrojovka, A.S., Sig Sauer, Inc. and Sturm, Ruger & Co., Inc., as well as Israel Weapon Industries, LTD for the polygonal barrels. Emphasizing that these models of pistols belong to their owners and have no relationship with the authors, being selected for use worldwide, for academic and non-profit purposes only.

Numerical analysis

Two types of numerical analysis were performed using Ansys® software. CAD models were made respecting the measures of the free-flight area and the original breech bolt distance. All systems were analyzed in three dimensions, without using the symmetry tool, since the internal configuration of the barrel is asymmetric in longitudinal segments.

First, the pressure inside the barrel tube was determined by the Finite Volume Method (FVM). The Fluent[®] module was used with a pressure-based solver for combustion and chemical species transport. The total length of the hexagonal and groove modeled barrels was 200 mm, according to the dimensions of the standardized barrel. The pressure is obtained in the chamber, in the same location where it is experimentally measured in standardized barrels, which have a slot 21 mm from the rear of the barrel, in which a piezoelectric transducer is located to measure the pressure.^{22–24} In this case, a turbulent flow regime and the Eddy-dissipation model is considered, being expressed by:^{15,25}

$$R_{i,r} = v'_{i,r} M_{w,i} A \rho \frac{\varepsilon}{k} \min R \frac{Y_R}{v'_{R,r} M_{w,R}} \quad (1)$$

$$R_{i,r} = v'_{i,r} M_{w,i} A B \rho \frac{\varepsilon}{k} \frac{\sum_P Y_P}{\sum_j v''_{j,r} M_{w,j}} \quad (2)$$

where i , is the net rate of production of species due to the r reaction; $R_{i,r}$ is given by the smaller limiting value of the equations (1) and (2); Y_R is the mass fraction of a particular R reactant; Y_P is the mass fraction of any product species P ; A and B are empirical constants equal to 4 and 0.5, respectively.

For the transport of species, the smokeless double-base powder combustion was considered, performing the calculations of the chemical reaction with the ICT-Thermodynamic-Code[®]. The properties of density, heat capacity, and enthalpy of the components of this gunpowder, such as nitrocellulose (13.25% N), nitroglycerin, potassium nitrate, centralite, and ethanol, were considered.

Ten analyzes were carried out on each barrel, progressively increasing the position of the projectile inside it. The first analysis was carried out with a barrel length of 25 mm, which corresponds to the position of the bullet when exceeded by 4 mm the position of the piezoelectric transducer slot. The eight subsequent analyzes were carried out with 20 mm increments in the bullet position and the last one of 15 mm, to reach the final length of the barrel 200 mm. This procedure is described in detail by Silva-Rivera et al.¹⁵

Besides, the conditions of the system were specified, such as the specific heat ratio at 1.2105, the density of the double base powder of 210 kg/m³, the stagnation temperature of 2200°K, and the maximum chamber pressure of 230 MPa, according to the STANAG-4090 standard.²²

The second type of numerical analysis was performed with the Finite Element Method to obtain Velocity, Deformation depth, Deformation width, Equivalent Plastic Strain, and Equivalent Stress. In this case, the initial total length of the two modeled barrels was also 200 mm, as in the FVM case. However, to reduce the computation time, these models were simplified, removing the case of the cartridge and the corresponding part of the chamber. Then the barrel was left with a length of 182.00 mm and a rifling length of 177.50 mm. This to obtain the same experimental pressure results, which cannot be obtained with gun barrels without being drilled.

Bullets were modeled with a length of 15 mm and their maximum diameter was located at 4.50 mm before the beginning of the rifling. The Transient Thermal[®] and Explicit Dynamics[®] modules were solved linked since it a firing time close to 2 ms. The primary method used was the displacement of the bullet within the barrel, which is given by the equation of a dynamic system as:^{12,26}

$$M\ddot{U} + C\dot{U} + KU = F \quad (3)$$

where M denotes the mass matrix; U is the displacement; \dot{U} is the velocity; \ddot{U} represents the acceleration; C is the damping matrix; K indicates the stiffness matrix; and F is the loading vector.

To calculate the contacts, the body interaction condition with penalty formulation was used. Indicating the projectile faces as the contact body and the internal faces of the barrel as the target body. Likewise, a friction coefficient of 1.4 was used, as determined by Deng et al.,¹² who also carried out stress-strain tests on projectiles caliber 9 mm in barrels with conventional rifling. The penalty method adds a normal contact force to avoid penetration, which is given by:^{12,26}

$$f_s = - l k_i n_i \quad (4)$$

Here, l is the penetration length; k_i is the contact stiffness; n_i is the unit normal vector of the surface contact element. The deformation undergone by the material is determined in the plastic regime by:^{12,26}

$$\frac{S_{ij} S_{ij}}{2} - \frac{\sigma_y^2}{3} = 0 \quad (5)$$

$$S_{ij} = \sigma_{ij} - \sigma_m \delta_{ij} \quad (6)$$

Where σ_y denotes the yielding stress; S_{ij} is the deviatoric stress tensor; σ_m is the spherical stress; and δ_{ij} is the Kronecker delta. The relationship with Young's modulus (E) is:^{12,26}

$$\frac{1}{E_t} = \frac{1}{E} + \frac{1}{E_p} \quad (7)$$

Where E_t is the tangent modulus; and E_p is the plastic modulus. AISI 4340 steel was assigned to the barrel, with a tensile yield strength of 250 MPa and Ultimate Tensile Strength (UTS) of 460 MPa. In the case of the projectile, a mass of 7.45 g was considered. The jacket is made of copper cast with a yield strength of 33.5 MPa and 152 MPa UTS. The core of lead-antimony with a yield strength of 13.7 MPa and 22.4 MPa UTS.

In all materials, conditions of nonlinear behavior, plastic strain failure and bilinear isotropic hardening were specified. Thus it was reasonably possible to obtain that the projectile could deform during its trajectory within the grooved and hexagonal barrel.

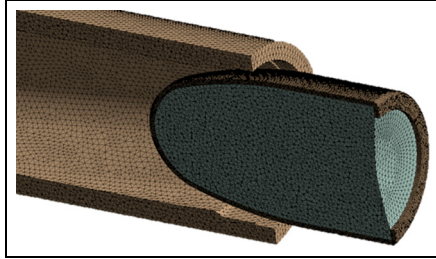


Figure 1. Meshed model (cut-away view) of the hexagonal rifling barrel.

In the FEM, a transient thermal analysis was first performed, using an initial temperature of 22°C that increases to 2200°C , and as a result of a conduction process, the temperature of the bullet rises to 612.6°C . Later, in the Explicit Dynamics analysis, the position of the barrel was fixed and the displacement of the bullet was established, with freedom in two of the axes (X and Y in this case).

In the Z component, the bullet displacement was specified with a maximum distance of 205 mm. Taking into account that its maximum diameter was initially 4.50 mm from the rifling, so the projectile in its final position exceeds the muzzle by 16 mm. This to identify the conditions at the beginning of the projectile's flight path. Moreover, this final position was located at 1.5 ms, the average time in which experimentally the projectile leaves a standardized 200 mm barrel.

Figure 1 shows the longitudinal section of the mesh of the hexagonal rifling barrel, observing in the part of the bullet its metallic jacket and its lead-antimony core. The free-flight area considered, and the start of the hexagonal rifling is also appreciated. Similarly, in Figure 2 the same 9 mm Parabellum bullet is observed, but in this case, inside a grooved barrel. In both cases, the position of the projectile is before it reaches the barrel rifling.

Meshing in both cases consisted of 0.1 mm elements for the metallic jacket, 0.3 mm for the core, and 0.3 mm for the barrel. Using tetrahedral elements with capture curvature and proximity.

Experimental analysis

Pressure and velocity tests were carried out first, three tests of 10 rounds each, using a standard barrel and a ballistic chronograph equipped with two optical barriers. MIL-C-70508²³ indicates an instrumental distance of 16 m, with speeds of $385 + 15$ m/s. In contrast, the SAAMI specification²⁴ indicates an instrumental distance of 4.57 m (15 Δ), but for different weights of 9 mm bullets, ranging from 5.70 g (88 gr) to 9.52 g (147 gr), and with velocity ranges from 300 to 457 m/s. For this reason, it was chosen to use a single type of bullet, standardizing its weight at $7.90 + 0.1$ g (122 + 1.54 gr) for all pressure and velocity tests, obtaining velocities of 340 m/s.

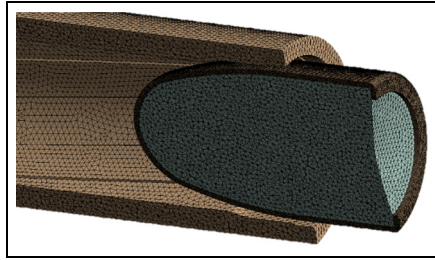


Figure 2. Meshed model (cut-away view) of the groove rifling barrel.

The second type of test was only of velocity, using the indicated weapons, the standardized 7.90 g bullet, and the MIL-C-70508.²³ Also, in this case, three tests of 10-round each were carried out with all pistols, indicating the average values in the results. In addition to the velocity measurements at 16 m, the ballistic chronograph also provides results at the muzzle, which were compared with those obtained by numerical simulation.

The third experimental test corresponds to the dimensional measurements of the weapons barrels and the fired projectiles, using a stereoscopic microscope model Velab VE-S5. For these tests, 30 rounds were fired by each gun, in series of 10 rounds with ammunitions of 7.45 g (115 g), 7.90 g (122 gr), and 8.03 g (124 gr). The projectiles were collected, and the rifling impression was measured. It is essential to highlight that this test aimed to determine the width of the grooves and the lands caused by both barrels. This is different from the method used in forensic studies, in which each trace of the rifling impression is analyzed with comparison microscopes and with automatic ballistic identification systems such as FIREBALL, IBIS or EVOFINDER, which help investigators find similarities between fired bullets and cartridge cases^{19–21} automatically.

Results

Pressure

The results of the experimental tests carried out allowed us to correctly characterize the ballistic behavior of the firing of 9 mm × 19 mm ammunition in hexagonal and grooved rifling barrels. Likewise, an acceptable correlation was obtained with the results of the numerical simulations. The results of the pressure tests are shown in Figure 3. The curve called “Experimental grooving” corresponds to one of the shots fired into the standardized test barrel, which was selected to coincide with the average value of 172 MPa. This average pressure value was obtained from 3 tests of 10-round each.

In this study, it was not possible to obtain an experimental pressure curve for a hexagonal barrel, since there is no agreement to standardize a polygonal test barrel. The pressure curves obtained by numerical analysis are also presented for firing in

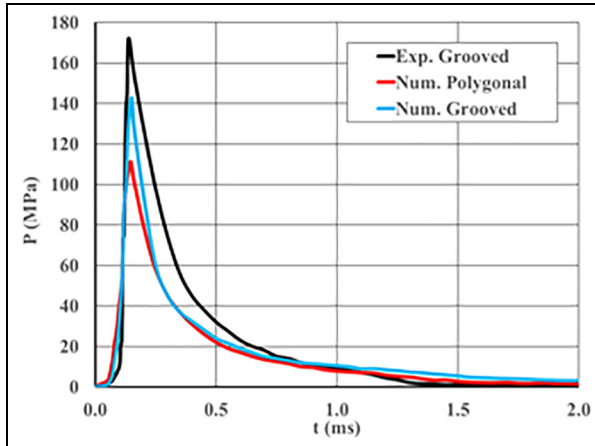


Figure 3. Average pressure curves of 9 mm shots in the barrel chamber.

a grooved barrel, called “Numerical grooving,” and in a polygonal barrel indicated as “Numerical polygonal.”

In this case, the experimental curve does not show a first pressure peak from the primer ignition, unlike the pressure tests carried out by Silva-Rivera et al.^{14,15} to 7.62 mm × 51 mm cartridges. This is because 9 mm × 19 mm ammunition has a lower volume inside, with a powder charge of 0.30 g, so it is ignited entirely by the primer, reaching maximum pressure simultaneously. As mentioned, the maximum value of this experimental pressure curve is 172 MPa at 0.14 ms, which is below the maximum allowable pressure in the chamber 215 MPa indicated by MIL-C-70508 standard²³ and also complies with the 230 MPa of the maximum pressure of the STANAG-4090 standard.²²

Besides, it is observed that the numerical simulation curves are similar, obtaining in the case of the grooved barrel a maximum pressure of 143 MPa at 0.15 ms, and in the hexagonal barrel a maximum pressure of 111 MPa at 0.14 ms. Which also meets with the indicated in the previous standards. It can be considered that the numerical results are low; however, experimental values up to 90 MPa were obtained, with velocity values within the range of the above standards. Therefore, the numerical values obtained are within this range of experimental results.

Velocity

In the same previous pressure tests, the velocity values corresponding to the grooved test barrel were also obtained. In addition, only velocity tests were carried out with three series of 10-round in each of the weapons described in Table 1, as specified in the MIL-C-70508 standard.²³

Table 2 shows the average values of the tests carried out for weapons with polygonal barrel and Table 3 for weapons with a conventional barrel. The comparison

Table 2. Velocity results in 9 mm pistols with polygonal rifling barrel.

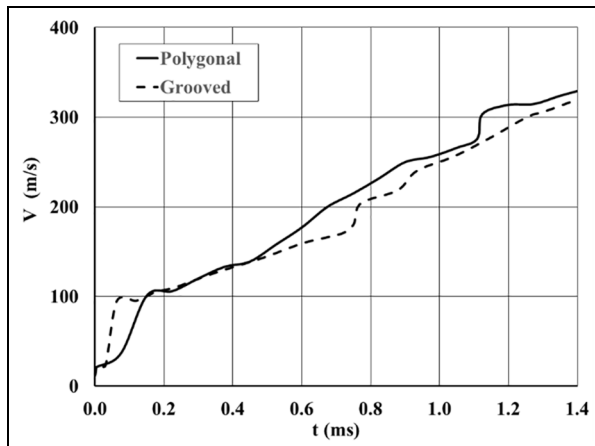
Mean velocity	IWI Jericho	IWI Masada	IWI Masada	Numerical
Muzzle	323	324	327	332
Inst at 16 m	317	318	321	N/A
Std. dev.	8	10	6	N/A
High value	341	336	325	N/A
Low value	316	299	308	N/A

N/A: not applicable.

Table 3. Velocity results in 9 mm pistols with groove rifling barrel.

Mean velocity	Sd barrel	CZ P09	SS P320	Ruger P89	Numerical
Muzzle	344	324	324	316	322
Inst at 16 m	336	318	318	311	N/A
Std. dev.	3	7	9	8	N/A
High value	341	336	333	329	N/A
Low value	329	313	298	298	N/A

N/A: not applicable.

**Figure 4.** Velocity curves of 9 mm shots.

with the numerically obtained values is only at the muzzle, indicating the experimental values at an instrumental distance of 16 m as a reference.

Figure 4 shows the velocity of the projectile inside the barrel plotted against time. The curves were obtained numerically and correspond to the firing in both barrels, in both cases with a length of 200 mm. It is observed that the two curves

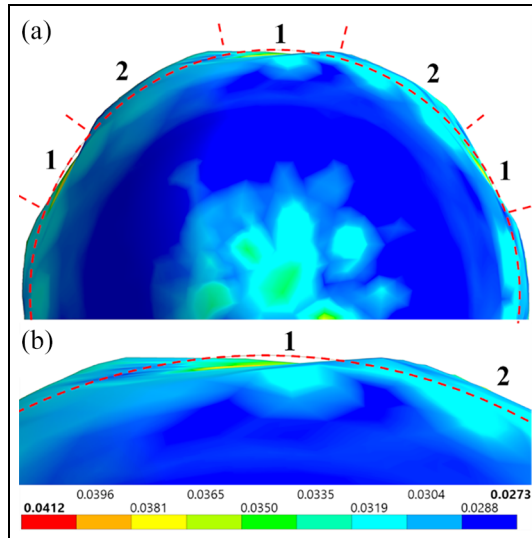


Figure 5. Front view of 9 mm deformed bullet in a hexagonal rifling barrel: (a) middle section and (b) upper part.

are similar to proportional growth until reaching the output velocity of 332 m/s in the muzzle for the polygonal barrel and 322 m/s for the conventional barrel. These values are consistent with the 344 m/s obtained experimentally. Some discontinuities in the growth of the curves are also observed, which correspond to the friction and the thrust that the projectile undergoes during its path.

Deformation depth

With the Finite Element Method described, the equivalent plastic strain that occurs in the projectile through the barrel was obtained. The front view of the numerically deformed projectile after its exit from the polygonal barrel is shown in Figure 5. It corresponds to the Equivalent Plastic Strain analysis, with a color scale for the magnitudes from 0.0273 to 0.0412 mm/mm. According to the experimental measurements, the hexagonal barrel has a minimum distance of 8.70 mm on the sides of the hexagon. Therefore, considering the maximum diameter of the Parabellum bullet of 9.017 mm, an interference fit is generated during its trajectory.

Figure 5(a) corresponds to the middle section of the projectile, highlighting in its outline a red dotted line that represents the original diameter of the Parabellum bullet before deforming. Figure 5(b) is a detail of one of the six sides of the projectile deformed towards its interior. The inward deformation zones are indicated with the number 1, the maximum deformation, in this case, being 0.158 mm on each side, with an approximate deformation width of 2.86 mm on each of the six sides. Also, two of the six segments are observed that are deformed outwards,

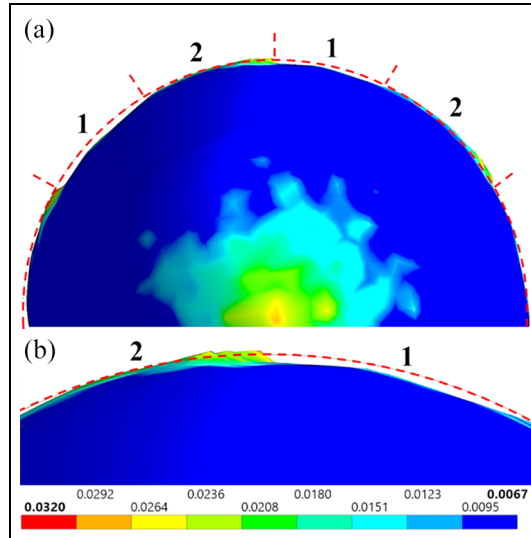


Figure 6. Front view of 9 mm deformed bullet in a groove rifling barrel: (a) middle section and (b) upper part.

indicated by the number 2, with a height of 0.178 mm with a width of 1.85 mm, which is observed. These segments are transition areas and exceed the original diameter of the projectile because, in the hexagonal barrel, its sides are joined by round fillet and not at 90° angles as in a geometric hexagon figure. So the chamber diameter is not exceeded. However, if there is an amplitude in the maximum diameter of the barrel, so the projectile is deformed outward in those areas due to the pressure and temperature generated.

The case of the numerically deformed projectile in a groove rifling barrel is seen in Figure 6. Again, the images correspond to the Equivalent Plastic Strain, with a color scale for the magnitudes obtained ranging from 0.0067 to 0.0320 mm/mm.

The middle section of the projectile is shown in Figure 6(a), and similarly has a dotted red line indicating its original diameter. These results were obtained considering in the model the maximum diameter of the Parabellum bullet and the minimum dimensions of the grooved barrel indicated in the STANAG-4090 standard.²² Again, it was determined that there is an interference fit. The inward deformations are shown in Figure 6(b), caused by the penetration of the barrel hills with a depth of 0.112 mm each, indicated with the number 1. As observed, there is a greater displacement of the volume in the central part of the image, which corresponds to the right side of the hill. This can be seen in more detail in the analysis of the rifling impressions left in the bullets fired in groove rifling barrels in Figure 6.

Even under these conditions, there is a clearance between the barrel grooves and the bullet of just 0.011 to 0.024 mm, part of these areas being deformed outwards and indicated by the number 2. In the left part of Figure 6(b) a segment of the

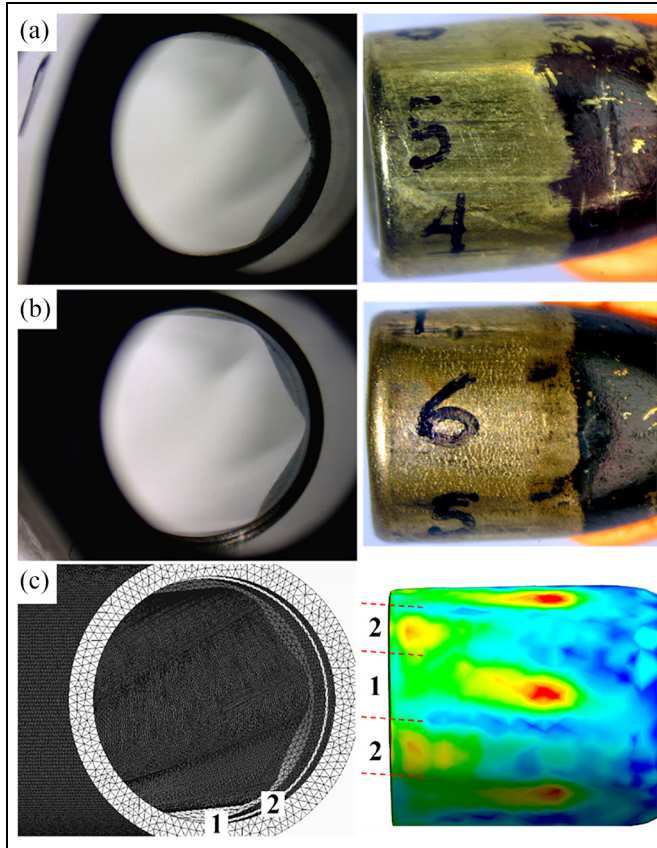


Figure 7. Polygonal barrels and detail of rifling impressions on bullets: (a) IWI Jericho, (b) IWI Masada, and (c) numerical polygonal barrel.

deformation towards the outside is observed. That is the volume of the bullet that moves outward in the clearance that exists between the diameter of the projectile and the grooves or valleys of the barrel.

Deformation width

The fired bullets were obtained, and the deformation generated by the polygonal and grooved barrels was measured using the third type of experimental tests. Figure 7 compares the projectiles obtained experimentally with the two kinds of polygonal guns used, as well as the barrel and the projectile obtained numerically. This makes it possible to visualize the rifling impression left on the projectiles by the hexagonal barrels. Figure 7(a) shows the IWI Jericho barrel with an obtained bullet of 7.45 g (115 gr), Figure 7(b) corresponds to the IWI Masada barrel with an

8.03 g (124 gr) bullet, and Figure 7(c) shows the meshed barrel with the equivalent plastic deformation of the projectile, which has the same magnitudes described above. The number 1 indicates one of the lands or hills in the barrel, which corresponds to the maximum protuberance on that side of the hexagon, as well as one of the striations generated in the projectile. Similarly, the number 2 indicates one of the valleys of the cannon, as well as the striations generated in the projectile.

Bullets were marked with indelible ink on their surface to have a better view of the experimental results since the impressions rifling are lesser than those of the conventional barrel striatum.¹⁹⁻²¹ The barrels had to be tilted at 3° to improve the perspective of at least three sides of the hexagon, and the images correspond to the rear part in the guns' chamber, focusing on the beginning of the hexagonal rifling segment.

Similarly, in Figure 8 the conventional barrels with the ammunition obtained are shown, observing the rifling impressions left by the grooves and lands. In this case, the barrels are seen in their front part in the muzzle, amplifying the end of the rifling, which in all cases corresponds to six grooves. Figure 8(a) shows the barrel of the CZ P-09 pistol and an 8.03 g (124 gr) bullet; Figure 8(b) shows the barrel of the Sig Sauer P320 with a bullet of 7.45 g (115 gr); Figure 8(c) the barrel of the Ruger P89 with an 8.03 g (124 gr) bullet; and in Figure 8(d) the barrel modeled with the deformed bullet by numerical simulation. It is indicated with the number 1 one of the lands or hills of the barrel, and the fluted generated in the projectile. Also, the number 2 indicates one of the valleys of the barrel, as well as two of the six striations generated in the projectile.

By measuring the rifling impressions of all the projectiles fired in these tests, the ranges of average values were obtained. Table 4 shows the measurements of the projectiles fired in polygonal barrels, and Table 5 shows those fired in grooved guns. In both cases, the values obtained experimentally and numerically of the width of the rifling impressions are indicated. The rifling produced by the hills or lands generates a deformation towards the interior of the projectile, which was only possible to size numerically, indicating the corresponding values. Likewise, in the valleys of the barrel, there is a deformation in the projectile towards the outside, having also dimensioned using numerical simulation, and its value is indicated with a negative symbol concerning the deformation in depth. Finally, analyzing the numerical results, it is observed that the values are within the ranges obtained experimentally for the polygonal barrel and grooved barrel.

Equivalent plastic strain

Figures 9 and 10 show the comparison of the deformation undergone by the bullet inside the hexagonal barrel. Figure 9 shows an 8.03 g (124 gr) bullet obtained experimentally in a hexagonal barrel, and Figure 10 shows the numerically deformed bullet after its exit from the muzzle. It is noted that lateral deformations are not complete due to the radial shape of the projectile is not completely transformed into a hexagon form. Instead, there are transfer spaces between each side,

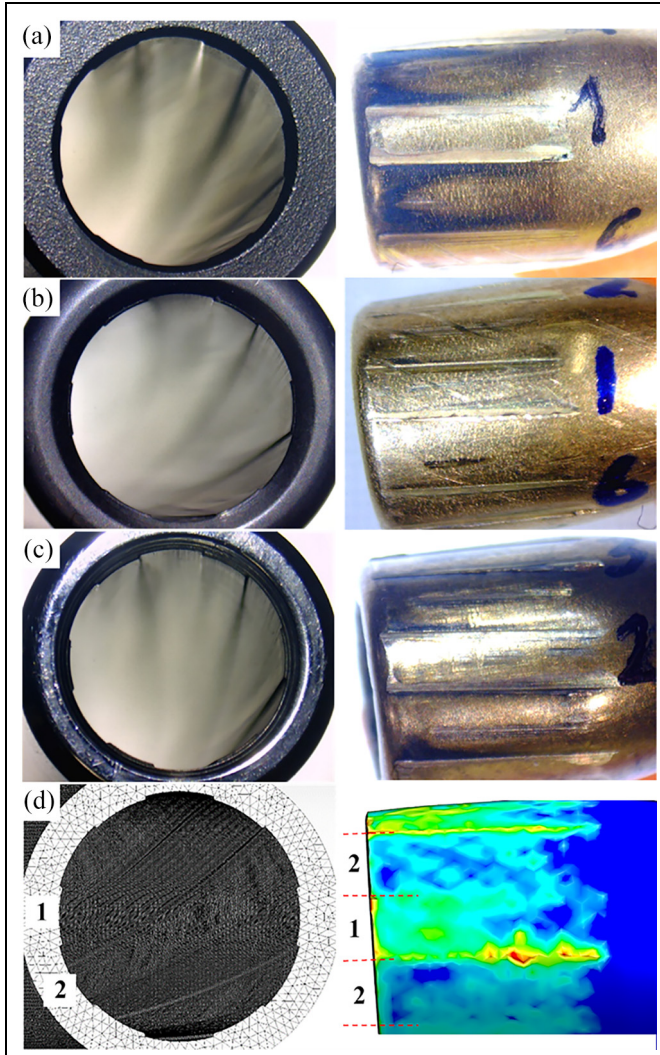


Figure 8. Grooved barrels and detail of rifling impressions on bullets: (a) CZ P-09, (b) Sig Sauer P320, (c) Ruger P89, and (d) numerical grooved barrel.

which have a width between 1.80 and 1.90 mm. The numerical result corresponds to the equivalent plastic strain with ranges from 0.0273 to 0.0412 mm/mm.

In the case of the groove rifling barrel, Figure 11 shows the rifling impressions of the barrel hill on a bullet. The result obtained by experimental tests is shown in Figure 11(a), where the hill produces a deformation of 1.80 to 2.10 mm width on the bullet. This result verifies that obtained through the numerical simulation of 2.04 mm width with a penetration depth of 0.112 mm shown in Figure 11(b), and

Table 4. Rifling impressions on 9 mm bullets fired from polygonal barrels.

Location	Polygonal barrel			
	IWI Jericho	IWI Masada	FEM width	FEM depth
Barrel's groove	1.53–1.85	1.65–1.83	1.85	−0.178 ¹
Barrel's land	2.74–2.87	2.80–2.90	2.86	0.158 ²

¹Maximum expansion height from the original circumference.

²Maximum depth of penetration from the original circumference.

Table 5. Rifling impressions on 9 mm bullets fired from grooved barrels.

Location	Grooved barrel				
	CZ P09	Sig Sauer P320	Ruger P89	FEM width	FEM depth
Barrel's groove	2.48–2.70	2.46–2.65	2.47–2.73	2.48	−0.025 ¹
Barrel's land	1.80–2.00	1.88–2.05	1.80–2.10	2.04	0.112 ²

¹Maximum expansion height from the original circumference.

²Maximum depth of penetration from the original circumference.

**Figure 9.** Deformed (experimentally) 9 mm bullet in a hexagonal barrel.

which corresponds to the equivalent plastic strain ranges from 0.0067 to 0.0320 mm/mm.

In both images, the greatest deformation is observed in the lower area of the rifling impression by the land or hill. This area coincides with the right side of each hill, seen from the chamber of the barrel. Therefore, in the barrel with a right-hand twist, greater wear is produced on this side than on the opposite side.

The comparison of equivalent plastic strain between the projectiles fired in the two types of guns is shown in Figure 12. The bullet fired in the polygonal barrel is shown in Figure 12(a), identifying that the main deformation point is in the center

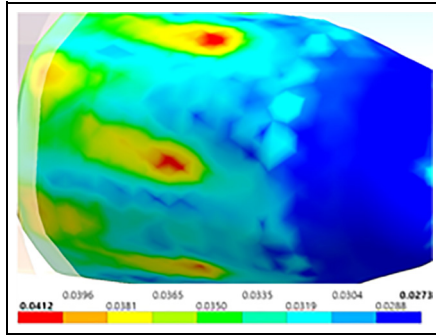


Figure 10. Deformed (numerically) 9 mm bullet in a hexagonal barrel.

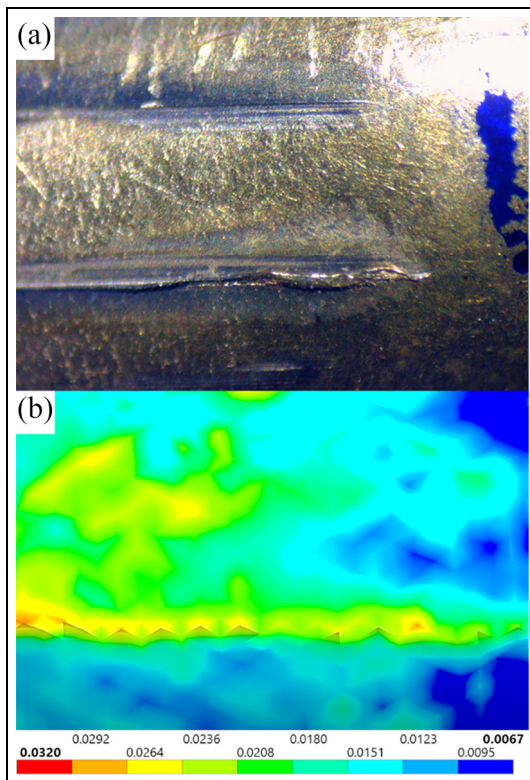


Figure 11. Rifling impression left by groove rifling barrel: (a) experimentally and (b) numerically.

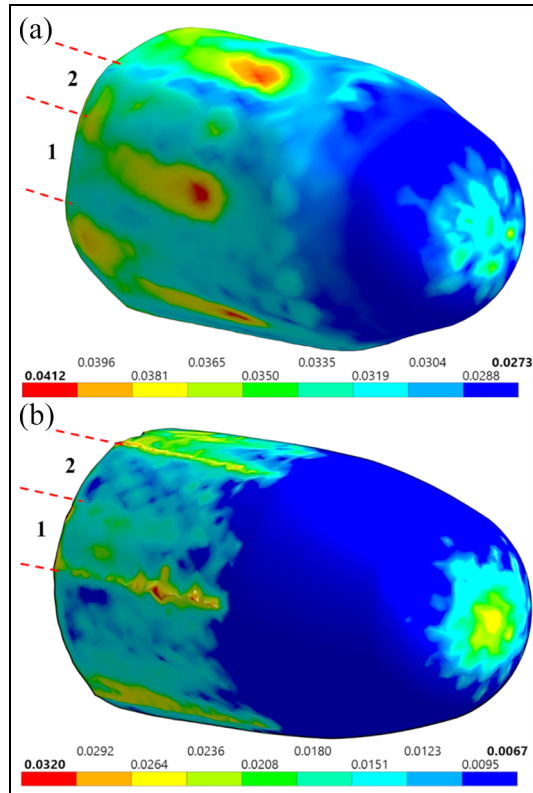


Figure 12. Equivalent plastic strain (mm/mm): (a) polygonal barrel and (b) grooved barrel.

of each of the sides, indicating one of them with the number 1, as well as one of the transition areas that deform outwards with the number 2. The magnitudes range from 0.0273 to 0.0412 mm/mm, so the deformation in the depth of 0.158 mm and towards the outside of 0.178 mm previously determined coincide with this range.

Similarly, the result for a projectile fired in a groove rifling barrel is shown in Figure 12(b), observing the deformation that occurs in the bullet by at least three lands or hills, and marking one of them with the number 1, with values from 0.0067 to 0.0320 mm/mm. This coincides with the penetrated depth values of 0.112 mm in each of the six hills. It is also indicated with the number 2, one of the six areas that correspond to the groove of the barrel.

For both types of barrels, the equivalent plastic strain curves against time are plotted in Figure 13. As indicated above, it is observed that the bullet undergoes a greater deformation in the polygonal barrel, and a greater area compared to the deformation of a projectile in a grooved barrel.

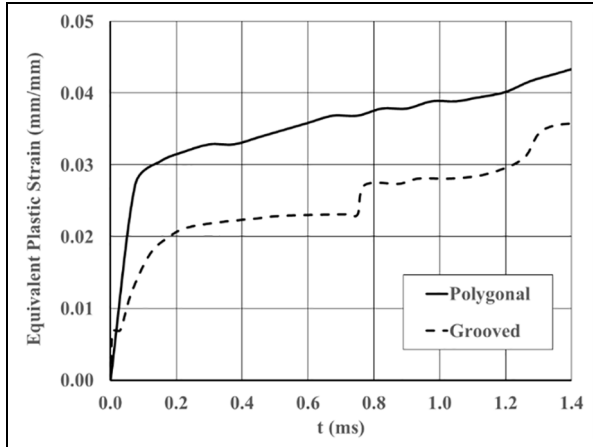


Figure 13. The plastic strain on 9 mm bullets.

Equivalent stress

The equivalent stress of the 9 mm bullet in a polygonal barrel is observed in Figure 14(a). The values were determined from 4.14 to 295.85 MPa, observing that the maximum stress values are presented in the areas of flat deformation that correspond to each of the six sides of the hexagon. The case of a projectile fired into a grooved barrel is shown in Figure 14(b), with values from 2.82 to 269.79 MPa. It is verified that greater stress on the bullet is produced by the right side of the hill seen from the chamber of the barrel. It is also observed that the greatest stress occurs in both cases at the rear of the projectile, at the end of the brass jacket, and its union with the core.

The behavior of these stresses against time inside the barrel is observed in Figure 15. It identifies that the maximum values exceed the ultimate tensile strength at 270 MPa, for an annealed red brass that is the material of the bullet jacket. However, this only happens for a fraction of a millisecond; thus, the bullet only deforms within its plastic regime without cracking. This considering the temperature and pressure of the system, as well as that the projectile is contained within the walls of the barrel tube.

Conclusions

In this research, the ballistic behavior of 9 mm bullets in polygonal barrels and grooved barrels was determined. First, the critical dimensions in both types of guns and their effects on the projectiles were identified. Then numerical analyzes were performed using the Finite Volume Method and the Finite Element Method, obtaining parameters of pressure, velocity, deformation, strain, and stress, which was corroborated with experimental tests.

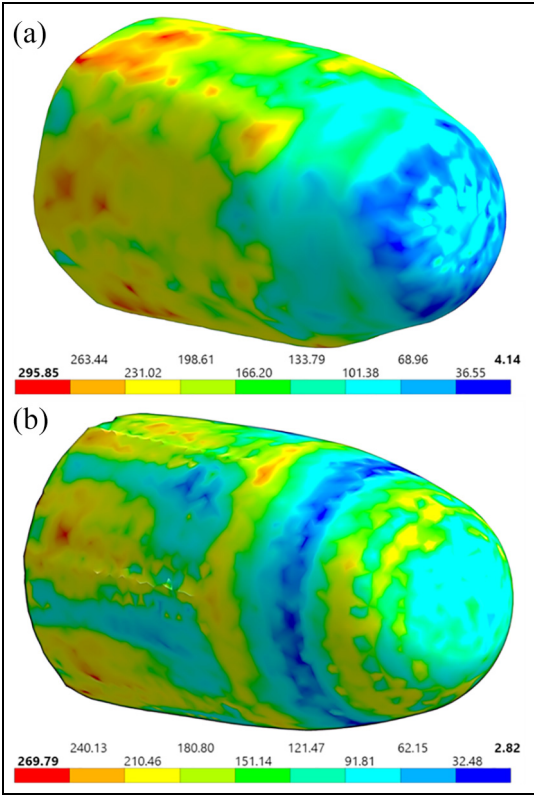


Figure 14. Equivalent stress: (a) polygonal barrel and (b) grooved barrel.

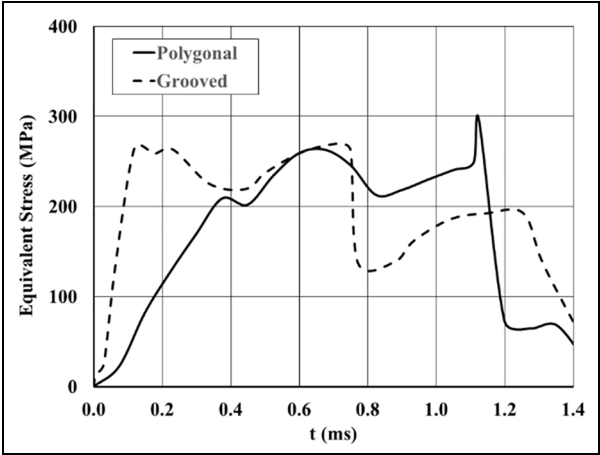


Figure 15. Equivalent stress on 9 mm bullets.

Through the results, it was determined that there is no significant difference in the pressure and velocity of the shots fired in each type of gun. Variations in these parameters are more caused by the length and wear of the barrel than by the type of rifling. And it must be considered that there are also important variations due to the type of ammunition used, since there is a wide diversity with variations mainly in their weight, even when this study was limited to the 9 mm × 19 mm caliber of Full Metal Jacket type.

It was established that the projectiles fired in hexagonal barrels undergo deformations towards the outside and inside. Each land on the six sides of the polygonal barrel produces a maximum penetration of 0.158 mm in its central part, with a width of 2.86 mm. It was also determined that there is a transfer area in which the projectile is deformed outward 0.178 mm at its center, with an approximate width of deformation of 1.85 mm.

On the other hand, the projectile fired in a grooved barrel undergoes a deformation towards its exterior, but only until reaching the maximum clearance between the original diameter of the bullet and the groove or valley of the barrel, which is only 0.025 mm. In comparison, the barrel hills penetrate up to 0.112 mm each, with a maximum width of 2.04 mm. It was also corroborated that in groove rifling barrels, only the right edge of the hill produces greater penetration. This implies that this part of the hill will be the first to wear down over the life of the barrel.

These data can serve as a basis for the standardization of hexagonal barrels and the establishment of standards, making it possible to carry out subsequent studies of wear on these types of barrels.

Acknowledgements

Authors acknowledge the Autonomous University of Mexico State, the National Council of Science and Technology (CONACYT), and Mexican Military Industrial Engineers (Class of 2015-2021) for their contribution to the development of this academic research.

Author contributions

U.S.S.R. developed the numerical simulation aspects of this research, carrying out the CAD models and using the F.V.M. and F.E.M. L.A.Z.A provided the initial formulation of the project, methodology, did exhaustive work on reviewing, editing, and supervised this research. A.H.V.G. did thorough work on identify improvements, proposing test equipment, reviewing, and editing the paper. P.A.T.M., created the mathematical model and wrote the first draft of this paper. All authors participated in reviewing and writing of this manuscript. W.D.W.A. performed the experimental ballistic tests on standardized barrels and conventional weapons, analyzing and comparing these results with those obtained theoretically.

Declaration of conflicting interests


The author(s) declared no potential conflicts of interest with respect to the research, authorship, and/or publication of this article.


Funding


The author(s) disclosed receipt of the following financial support for the research, authorship, and/or publication of this article:

This research was funded by CONACYT (Consejo Nacional de Ciencia y Tecnología) Grant No. 2019-000006-01NACV-00861.

ORCID iDs

Usiel S Silva-Rivera  <https://orcid.org/0000-0001-5597-1638>

Luis A Zúñiga-Avilés  <https://orcid.org/0000-0002-4365-8537>

Pedro A Tamayo-Meza  <https://orcid.org/0000-0001-8026-8928>

References

1. Ozmen D, Kurt M, Ekici B, et al. Static, dynamic and fatigue analysis of a semi-automatic gun locking block. *Eng Fail Anal* 2009; 16: 2235–2244.
2. Liu F-f, Song Y-m, Yu H-l, et al. Study on the influence of projectile on muzzle disturbance. *Def Technol* 2018; 14: 570–577.
3. Dursun T, Büyükcivelek F and Utlu Ç. A review on the gun barrel vibrations and control for a main battle tank. *Def Technol* 2017; 13: 353–359.
4. Tiwari N, Patil M, Shankar R, et al. Rigid body dynamics modeling, experimental characterization, and performance analysis of a howitzer. *Def Technol* 2016; 12: 480–489.
5. Jiang XH, Fan BC, Li HZ, et al. Numerical investigations on dynamic process of muzzle flow. *Appl Math Mech* 2008; 29: 351–360.
6. Xue T, Zhang Xb and Cui Dh. Dynamic analysis of a guided projectile during engraving process. *Def Technol* 2014; 10: 111–118.
7. Procházka S and Ninh ND. Differences in barrel chamber and muzzle deformation during shot. *Adv Mil Technol* 2012; 7: 77–89.
8. Lee HL, Yang YC, Chang WJ, et al. Estimation of heat flux and thermal stresses in multilayer gun barrel with thermal contact resistance. *Appl Math Comput* 2009; 209: 211–221.
9. Deirmenci E and Hüsnü Dirikolu M. A thermochemical approach for the determination of convection heat transfer coefficients in a gun barrel. *Appl Therm Eng* 2012; 37: 275–279.
10. Abhilash P and Chopade MR. Analysis of heat transfer coefficient inside gun barrel. *Int J Curr Eng Technol* 2011; 5: 460–463.
11. Suchocki C and Ewertowski J. Modeling and numerical simulation of semi-automatic pistol dynamics. *J Theor Appl Mech* 2015; 53: 81–91.
12. Deng S, Sun HK, Chiu CJ, et al. Transient finite element for in-bore analysis of 9 mm pistols. *Appl Math Model* 2014; 38: 2673–2688.
13. Taraszewski M and Ewertowski J. Complex experimental analysis of rifle-shooter interaction. *Def Technol* 2017; 13: 346–352.
14. Silva-Rivera US, Sandoval JM, Flores LA, et al. Numerical simulation and experimental study of flowfield around a bullet with a partial core. *J Appl Mech* 2011; 78: 1–5.
15. Silva-Rivera US, Sandoval-Pineda JM, Susarrey-Huerta O, et al. Numerical modelling of caseless ammunition with coreless bullet in internal ballistics. *Def Sci J* 2015; 65: 203–207.

16. Chinn GM. *The machine gun*, vol. IV. Washington, DC: U.S. Ordnance Bureau (Navy Department), 1955.
17. Glock GmbH. Gen 5 The next generation 2020, <https://eu.glock.com/en/technology/gen5> (accessed March 16, 2020).
18. Engel DR. *The truth about firearms and concealed carry*. USA: Trafford Publishing, 2014.
19. Banno A, Masuda T and Ikeuchi K. Three dimensional visualization and comparison of impressions on fired bullets. *Forensic Sci Int* 2004; 140: 233–240.
20. Fadul TG, Hernandez GA, Stoiloff S, et al. An empirical study to improve the scientific foundation of forensic firearm and tool mark identification utilizing 10 consecutively manufactured slides. *AFTE J* 2013; 45: 376–389.
21. Christen S and Jordi HR. Individuality testing of new Glock pistol barrels “Marksman Barrel.” *Forensic Sci Int* 2019; 295: 64–71.
22. International Standardization Agreement, *STANAG 4090 Small arms ammunition (9 mm parabellum)*. North Atlantic Treaty Organization, U.S.A. 1982.
23. Military Specification Cartridge, *MIL C 70508 (AR) 9 mm Ball NATO M882, Amendment 6*. U.S. Department of Defense, U.S.A. 1990.
24. SAAMI. *Voluntary industry performance standards for pressure and velocity of centerfire rifle ammunition for the use of commercial manufacturers*. Newtown, CT: SAAMI, 2015.
25. *ANSYS Fluent® theory manual*. Canonsburg, PA: ANSYS Inc., 2011.
26. *ANSYS LS-DYNA® theory manual*. Livermore, CA: Livermore Software Technology Corporation, 2006.

Author biographies

Usiel S Silva-Rivera is a Doctor in Mechanical Engineering (PhD) from the National Polytechnic Institute, Mexico. He is a Postdoctoral Researcher in the “Dynamics and Control Systems” research group of the Faculty of Engineering of the Autonomous University of the State of Mexico. His research interests are experimental ballistics, computational fluid dynamics (CFD), finite element method (FEM), materials, mechanical design, manufacturing, and quality control.

Luis Adrian Zuñiga Aviles is Doctor in Science and Technology on Mechatronics, He is a member of CATEDRAS CONACYT and the research group Dynamics and Control Systems of the Faculty of Engineering of the Autonomous University of the State of Mexico. He has been involved in research projects of New Product Development mechatronics design process, design methodologies, Robotic Exoskeletons for Rehabilitation and Motion Assist, design of mechanisms and machines, test benches, finite element method (FEM), kinematics modeling and simulation, wheeled mobile robots, manufacture technologies, and rapid prototypes.

Adriana H Vilchis-Gonzalez is a computer engineer from the Autonomous University of the State of Mexico (UAEM). She received the Doctor degree in Image, Vision and Robotics from the Polytechnic National Institute of Grenoble, France. Her research is oriented towards modeling and control of mechatronic devices for educational, medical robotics and rehabilitation robots with an emphasis on modeling and innovation of medical devices such as soft robots, tensegrity robots and exoskeletons.

Pedro A Tamayo-Meza is a research professor at the School of Mechanical and Electrical Engineering, Mexico (ESIME-IPN). He has a doctorate in Metallurgical and Technological Engineering from the USSR Academy of Sciences, Moscow, Russia, and a master's degree in mechanical engineering from the Faculty of Engineering of the University of Moscow, Russia. His professional research experience includes atomic force microscope analysis (AFM), solid state physics, and cryogenic mechanical treatment.

Wilbert David Wong-Angel is an associate research professor at the School of Mechanical and Electrical Engineering, Mexico (ESIME-IPN). He obtained his two doctorate degrees in Metallurgy and Mechanical Engineering from the National Polytechnic Institute, Mexico. His research focuses on the physical mechanics of materials, tribocorrosion, failure mechanisms, fatigue, and metallurgy.